Brownian dynamics of elongated particles in a quasi-two-dimensional isotropic liquid

Christoph Klopp, Ralf Stannarius, and Alexey Eremin
Otto-von-Guericke-Universität Magdeburg, Inst. for Experimental Physics, Dept. of Nonlinear Phenomena, 39016 Magdeburg, Germany
(Received 11 April 2017; published 20 December 2017)

We demonstrate experimentally that the long-range hydrodynamic interactions in an incompressible quasi-two-dimensional isotropic fluid result in an anisotropic viscous drag acting on elongated particles. The anisotropy of the drag is increasing with increasing ratio of the particle length to the hydrodynamic scale given by the Saffman-Delbrück length. The microrheology data for translational and rotational drags collected over three orders of magnitude of the effective particle length demonstrate the validity of the current theoretical approaches to the hydrodynamics in restricted geometry. The results also demonstrate crossovers between the hydrodynamical regimes determined by the characteristic length scales.

DOI: 10.1103/PhysRevFluids.2.124202

I. INTRODUCTION

Motion of particles and their hydrodynamic interactions are of paramount interest not only for fundamental physics, but also for its applications in chemistry and biology. Liquid membranes are essential constituents of living matter. The mobility of particles (inclusions) embedded in biological membranes is known to determine many cellular processes such as signal transduction, stimuli response, and sensing [1,2]. Self-assembly of membrane proteins can influence biochemical reactions and even allows cells to sense their shape [3]. Therefore, understanding of dynamics in membranes is of paramount interest. Membrane proteins and lipid rafts have often sizes significantly larger than the membrane thickness, and they can be viewed as macroscopic objects immersed in a continuous 2D fluid [1,2,4,5]. Earlier studies of the dynamics of such structures revealed discrepancies in the determination of the membrane viscosities if the motion was described by 3D hydrodynamics [6–8]. For instance, an overestimation of the viscosity up to two orders of magnitude was found in experiments using fluorescent probes and NMR techniques [7]. Quantitative experimental data are rather scarce. Active microrheology studies of isotropic poly(dimethysiloxane) (PDMS) films on a fluid substrate revealed an appreciable discrepancy between experiment and theory [9,10]. This discrepancy was partially attributed to the compressibility of the PDMS layer. Here, we use smectic freely suspended films, which are unique models of nearly incompressible quasi-two-dimensional (quasi-2D) fluids allowing variation of hydrodynamic parameters in a very broad range. Both in-plane isotropic (smectic A) and in-plane anisotropic (smectic C) fluid structures can be explored in this system.

An inclusion moving with the velocity $\mathbf{v}$ experiences the viscous force $\mathbf{F}$. The viscous drag coefficients $\zeta_{\alpha\beta}$ are given by the inverse mobility tensor, defined by the expression

$$\zeta_{\alpha\beta} v_\beta = F_\alpha, \quad \text{with } \alpha,\beta = x,y,z. \tag{1}$$

The viscous drag on a spherical inclusion in a viscous three-dimensional (3D) fluid at low Reynolds number is proportional to the radius of the particle (3D Stokesian regime). However, the situation in a 2D fluid is more complex. In the case of an infinitely extended membrane in vacuum, the mobility is expected to diverge (Stokes-Paradox). But as demonstrated by Saffman and Delbrück, the coupling between the flow in the membrane with the flow of the fluid or the fluids surrounding the membrane will result in a finite mobility, no matter how small the viscosities η', η'' of the outer fluids are [11]. The relation between the size of the inclusion and the drag force becomes a logarithmic function of the inclusion size. The coupling is described by a hydrodynamic length scale,

the Saffman-Delbrück length, $L_s = \eta_m/(\eta' + \eta'')$ defined as the ratio between the 2D membrane viscosity η_m and the 3D viscosities of the outer fluids η', η'' below and above the membrane, where $\eta_m = \eta h$ for a membrane with material viscosity η and thickness h [7,11–13]. For an inclusion with characteristic size L, L_s determines the Boussinesq number $\mathrm{Bo} = L_s/L$, which quantifies the relative contributions of the interfacial and bulk drag [10]. When the lateral dimensions of the membrane reach L_s or become smaller than L_s, coupling to the membrane boundary dominates and determines the dynamics of inclusions. Altogether, three different dynamic regimes can be distinguished: the 3D Stokesian regime, the 2D regime driven by the coupling to the outer fluid and the 2D regime governed by the lateral spatial constraints of the membrane. All those regimes were demonstrated experimentally for in-plane isometric inclusions (circular cross-section) [14,15]. In lipid membranes, depending on the membrane viscosities, both 3D and 2D dynamics have been reported [16]. Yet, in some cases, it was demonstrated that the continuous approach breaks down for small proteins, where the inhomogeneities of the membrane structure on a molecular scale may affect the protein diffusion [8].

However, often the shape of the inclusions cannot be assumed isometric and the problem of mobility of extended bodies in a 2D fluid must be considered in more detail [6,8,17,18]. Saffman [11] mentioned that the mobility of ellipses or ellipsoids can be easily calculated in a similar way as for discs. An example of this calculation is given in Ref. [18]. A rigid cylinder, perhaps one of the simplest anisometric shapes, exhibits distinctive hydrodynamical properties even in 3D fluids. Already in the limit of low Reynolds number, the purely local character of the hydrodynamic drag is broken. Viscous drag on a rod is anisotropic and exhibits a logarithmic length-dependence:

$$\zeta_{\parallel}^{3\mathrm{D}} = 2\pi\eta L\left[\ln\left(\frac{AL}{a}\right)\right]^{-1}, \tag{2}$$

$$\zeta_{\perp}^{3\mathrm{D}} = 2\zeta_{\parallel}^{3\mathrm{D}}, \tag{3}$$

where $\zeta_{\parallel}^{3\mathrm{D}}$ and $\zeta_{\parallel}^{3\mathrm{D}}$ are the drag coefficients for a motion parallel and perpendicular to the axis of the rod, respectively, L is the rod length, a is its radius, η is the dynamic viscosity of the fluid, and A is a numerical factor of the order of unity [19]. The topic of the present paper is an experimental study of the viscous drag and its dependence on the rod size in a 2D fluid. A theoretical model for the mobility of rod-shaped inclusions was put forward by Levine *et al.* [20]. They demonstrated that in contrast to the 3D case, the transverse drag coefficient $\zeta_{\perp}$ for larger rods becomes linear in length L, indicating that the viscous drag becomes purely local. In contrast, the parallel component $\zeta_{\parallel}$ of the drag for $L \gg L_s$ depends logarithmically on the length of the rod. At the same time, the relation in Eq. (3) breaks down in 2D. Rotational drag for rotation around the transversal axis in 3D is given by

$$\zeta_{\mathrm{R}\perp}^{3\mathrm{D}} = \frac{\pi\eta L^3}{3[\ln(L/2a) - C]}, \tag{4}$$

where C is a numerical factor which depends on the aspect ratio of the rod and is approximately 0.662 for infinitely thin rods [19,21].

In this paper, we study the mobility of anisometric rod-shaped particles in a freely suspended liquid crystal film by analyzing their Brownian motion. Variation of the length of the rods and the thickness of the film enables us to explore a wide range of hydrodynamic regimes determined by the ratios of the typical rod dimensions to the Saffman-Delbrück length L_s. We choose the commercial liquid crystal 4-n-octyl-4′-cyanobiphenyl (8CB), which exhibits the smectic-A phase at room temperature. Freely suspended films with thicknesses from few nanometers up to 5 μm were used in our experiments. The preferential orthogonal alignment of the 3.17-nm-long molecules without in-plane order at the film surfaces provides a unique opportunity to mimic a quasi-2D isotropic fluid. A sufficiently large extension of the film, in the range of a few centimeters, abates undesired boundary effects.

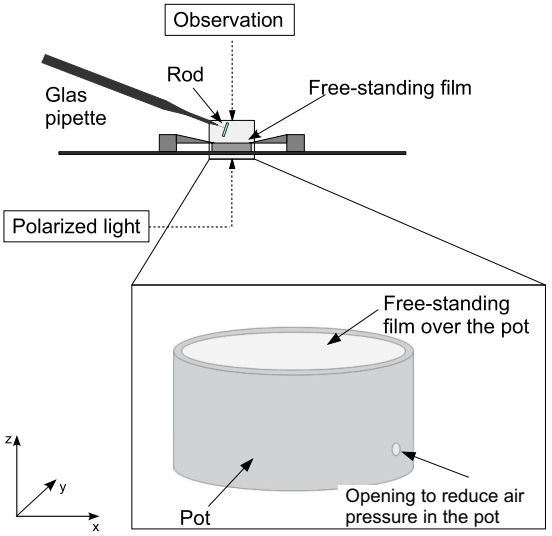

FIG. 1. Experimental setup for the study of Brownian motion in a freely suspended liquid crystal film. The film is drawn on an airtight sealed cylindrical container. Before deposition of the particles, we bend the smectic films lightly downward by an depression in the container, to avoid immediate drift of the particle into the meniscus. The pressure is then slowly equilibrated so that the experiment is performed with a flat film.

II. EXPERIMENTAL

The commercial liquid crystal 4-n-octyl-4′-cyanobiphenyl (8CB), which exhibits the smectic-A phase at room temperature and forms freely suspended films was used. The liquid crystal has a dynamic viscosity of $\eta = 0.052$ Pa s at a room temperature of $T = 22\,^{\circ}$C and is surrounded by ambient air with a viscosity of $\eta' = 1.8 \times 10^{-5}$ Pa s. The observations were made using an AxioScope Pol polarizing microscope (Zeiss GmbH). Glass rods of various lengths ranging from 60 to 1500 μm and widths of 10–20 μm were deposited on the film using a thin glass fibre attached to a micromanipulator [Figs. 1 and 2(a)]. The motion of the rods was video-recorded at the frame rate of 60 fps in color between crossed polarizers and the wave plate. In such experiments, a film of uniform thickness has uniform magenta color too, which can be easily subtracted to leave the rod surrounded by a meniscus of a thickness larger than that of the surrounding film. The rods with the surrounded immobile meniscus were tracked using standard Matlab particle tracking routines. The centroid and the axes of the particle in the film were determined for each frame. The particle image was fit with a rectangular shape with the axes collinear with the axes of the rod without meniscus. In this case, the boundary of the meniscus area determined the size of the particles. The sizes of single rods were determined from the microscopy images of a single rod. The particles were tracked on the time scale of 5 min. The mean-square displacement (MDS) was extracted using the procedure described in Refs. [14,15]. Translational and rotational drag coefficients were obtained from the MDS averaged over multiple trajectories. The relative measurement uncertainties of translation and rotational drag were estimated to be below 10%.

III. RESULTS

After deposition on the film, the glass rod is rapidly wetted by the LC material. A meniscus forms within about 3–5 s [Figs. 2(a) and 2(b)]. Polarizing microscopy reveals focal-conic textures in the meniscus [Fig. 2(a)], which indicates the presence of complex internal structures composed by layer dislocations and topological defects [22,23]. For this reason, the flow in the thick meniscus area cannot be considered as purely two-dimensional. The thickness in the meniscus increases fast

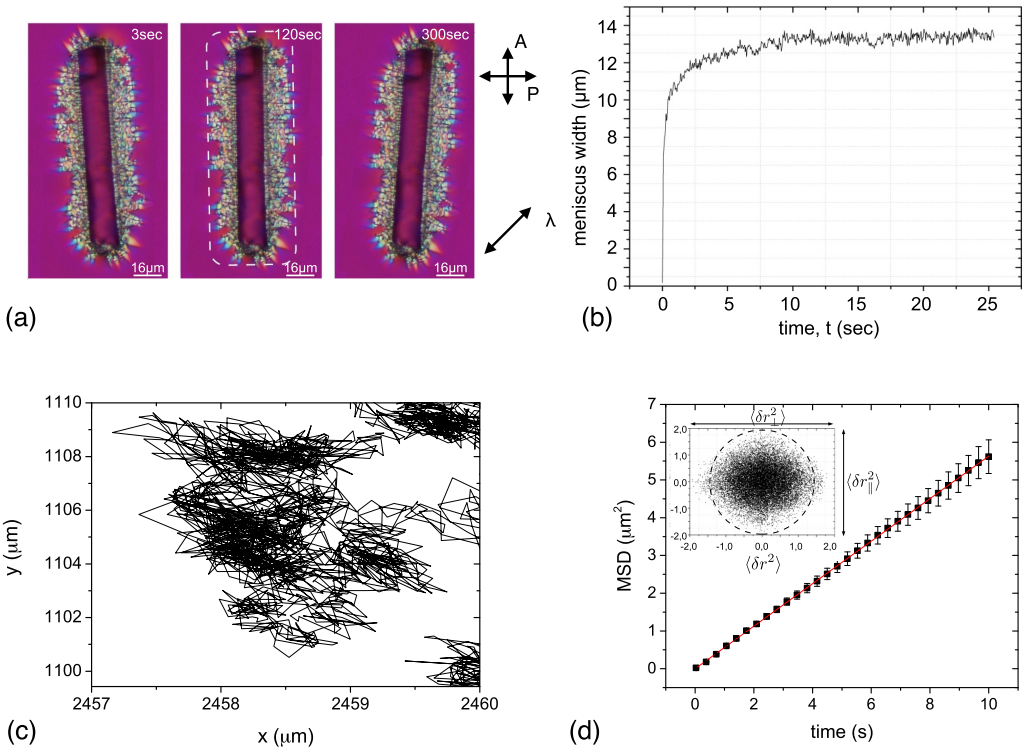

FIG. 2. (a) Polarizing microscopy images of a rod embedded in the freely suspended film, observed with a full wave plate. The images are taken at time instances of 3, 120, and 300 s after the deposition. The bright birefringent area of the meniscus indicates a complex inner structure where the smectic layers are deformed. Its boundary schematically marked by a dash line. The arrows on the right show the orientations of the polarizer P, analyzer A, and the wave plate λ. (b) Time dependence of the meniscus width for the rod in (a). (c) A fragment of a typical trajectory of a rod and (d) an example of the mean squared displacement MSD (drift-free) with a linear fit (solid line), in the inset, there is a distribution of displacements measured between positions on the trajectory separated by the time interval of 1/60 s.

with a distance from the film edge. So does the effective 2D viscosity, which is proportional to the thickness. In addition, layer dislocations in these patterns inhibit flow. Thus, the flow in the meniscus is substantially impeded by the internal structure of the meniscus, evidenced by the stationary optical textures. Consequently, we have to consider the meniscus area as immobile respective to the rod, and we introduce an effective dimension of the rod, by correcting it with the mean size of the meniscus:

$$L = L_{\mathrm{rod}} + 2L_{\mathrm{m}}, \quad W = W_{\mathrm{rod}} + 2W_{\mathrm{m}}, \tag{5}$$

where L_{rod} and W_{rod} are the length and the width of the bare glass rod, L_{m} and W_{m} are mean lengths and widths of the meniscus, respectively.

The Brownian motion of the rods was recorded over time intervals of 5 to 6 min, an example of such a trajectory is shown in Fig. 2(c). To determine the viscous drag ζ acting on the rod in a freely suspended film, we separate the Brownian motion from some unavoidable drift which impedes the measurement at long time scales. The separation of the two motions is achieved with a procedure described earlier [14]. The transversal and longitudinal components of the drag are obtained from the mean-squared displacement (MSD) relative to the rod axes, by separating the displacements parallel to the rod's momentary long and short axes [Fig. 2(d)].

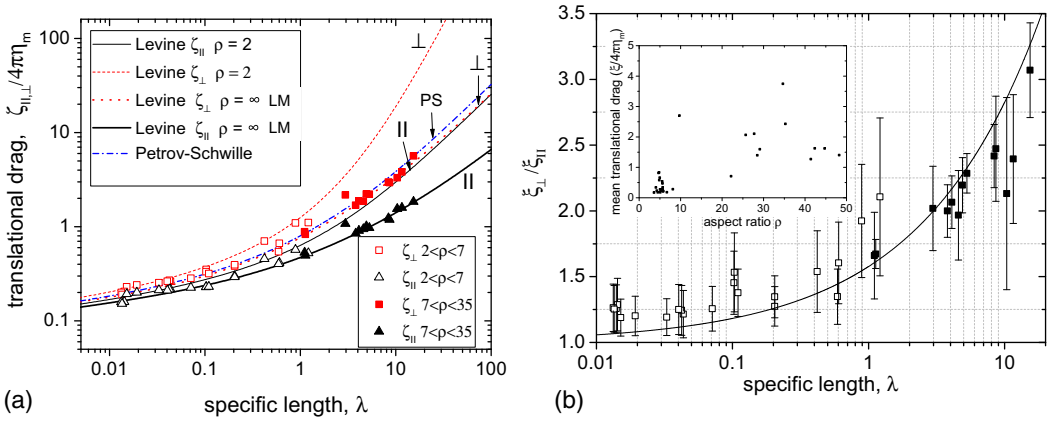

FIG. 3. (a) Parallel and perpendicular drag coefficients for thin rods as a function of their dimensionless length $\lambda = L/L_s$. The solid lines are theoretical predictions by the Levine model [24] for a rod aspect ratio $\rho = 2$ and for infinitely thin rods ($\rho = \infty$), (LM [24]). The dash-dotted line corresponds to the Petrov-Schwille equation with an argument $\lambda = L/L_s$ [13]. (b) Ratio of the perpendicular component of the viscous drag to the parallel component, $\zeta_\perp/\zeta_\parallel$ as a function of λ. The solid line is the theoretical prediction for thin rods from Ref. [24]. The experimental data points are separated in two groups of rods with different aspect ratios $\rho = L/W$: $2 < \rho < 7$ (open symbols) and $7 < \rho < 35$ (filled symbols). Due to only a small dispersion of the rod widths, the data points corresponding to small ρ occur at small λ. The dependence of the mean drag on the aspect ratio is shown in the inset of (b).

The experimental results for the translational drag coefficients in dependence on the effective rod length are shown in Fig. 3. Drag coefficients for different film thicknesses and rod lengths are scaled to the reduced rod length $\lambda = L/L_s$. The width of the rods including the meniscus is smaller than L_s in all cases. A first obvious result is that the diffusion along the rod axis, as expected, is faster than perpendicular to it. This feature is more pronounced when $\lambda > 1$. For $\lambda \approx 10$, a factor of about 2.5 is reached. The translational drag exhibits a distinct nonlinear behavior as a function of the reduced rod length. Approximating the rods by discs with the effective radius $R_{\text{eff}} = L/2$ [the mean radius $R_{\text{m}} = (L + W)/4 \to L/2$ for $W \to L$], and setting $\lambda = 2R_{\text{eff}}/L_s$, we can see that the experimental data for the mean translational drag $\zeta_m = 0.5(\zeta_\perp + \zeta_\parallel)$ cannot be satisfactorily approximated by the 2D drag model proposed by Petrov and Schwille (PS) as an extension of the Saffman-Delbrück theory for isometric particles (discs) [11–13]. The mean drag is systematically lower than the drag predicted by the PS model. Only for $\lambda \ll 1$, the experimental data are close to the PS prediction [Fig. 3(a)]. It is important to note that the PS drag in Fig. 3(a) is plotted as a function of L/L_s. In the case $\lambda \ll 1$, the aspect ratios $\rho = L/W$ of the rods used in our study are not large, and the mean radius is close to $L/2$. For larger λ, the drag coefficients for the displacements parallel to the rod axis, $\zeta_\parallel$, and perpendicular to it, $\zeta_\perp$, diverge from each other and the displacements become strongly correlated with the momentary rod axis. The transversal drag $\zeta_\perp$ becomes a linear function of the length λ. The parallel drag $\zeta_\parallel$ shows a slower continuous growth with λ.

IV. DISCUSSION

To calculate the drag on the anisometric particles in 2D, we followed the theoretical approach developed by Levine *et al.* [20,24,25], where velocity response functions parallel ($\chi_\parallel$) and perpendicular ($\chi_\perp$) to the rod long axis were used. Specific dimensionless drag coefficients $\zeta_{\parallel,\perp}/4\pi\eta_m$ were computed as functions of the reduced length λ using the Kirkwood approximations in Fig. 3(a). Two pairs of curves are included in Fig. 3(a): the theoretical dependencies $\zeta_{\parallel,\perp}/4\pi\eta_m$ for the rod aspect ratio of 2, computed using the Kirkwood approximation [19,25], and the thin-rod

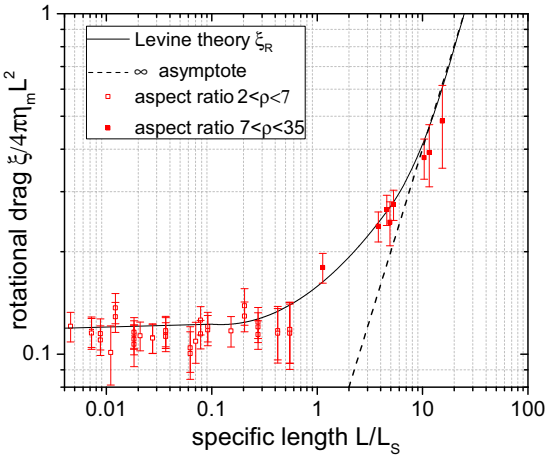

FIG. 4. Dependence of the rotational drag coefficient ζ_R on the specific length λ. The experimental data are compared with the prediction of the Levine theory [24] (solid line) for infinitely thin rods.

approximation from Ref. [24]. The fifth curve is the drag on a disk-shaped inclusion with radius $L/2$, computed using the Petrov-Schwille equation [13]. This curve covers both, the 2D Saffman-Delbrück regime for small λ and 3D Stokes regime for $\lambda \gg 1$.

The smallest value of L_s achieved in our experiment is about 40 μm, which is comparable with the widths of the rods used in our experiments ($W \approx 40$–45 μm). However, for thicker films, L_s significantly exceeds the width W. This justifies using the theoretical model for thin rods. In agreement with the theory by Levine *et al.* [25], even for thick rods, the translational drag coefficients become independent of ρ, and can be described in the thin-rod approximation, when λ is sufficiently small [Fig. 3(a)]. The plot in Fig. 3(a) shows an excellent agreement between the experimental drag and the theory for the 2D hydrodynamics. It is remarkable that no fitting parameters are used here. The anisotropy of the translational diffusion is already measurable for the shortest rods with the specific lengths, λ, as low as 0.01, and it increases with increasing length [Fig. 3(b)]. Even when $\lambda \ll 1$, the anisotropy of the viscous drag remains appreciable. The two curves for the transversal and longitudinal drag coefficients converge logarithmically. In the limit $\lambda \to 0$, the rod represents a singular distortion of the flow field and the structure of the rod on a scale much smaller than the Saffman-Delbrück length L_s becomes less important. The drag coefficients become nearly independent of the inclusion size and approach the values given by the PS formula [13] for isometric particles with a diameter of L in an isotropic membrane. This can be understood from the asymptotic behavior of the response functions, $\chi_\parallel$ and $\chi_\perp$, which leads to the Saffman-Delbrück drag force in the limit of small λ.

The rotational drag coefficient weighted by the length squared, $\zeta_R/4\pi\eta_m L^2$, is shown in Fig. 4. In agreement with the theoretical prediction by Levine *et al.* [20,24,25], the drag coefficient exhibits an algebraic dependence on the rod length in the asymptotic limits. It is proportional to λ^2 for $\lambda \ll 1$ and proportional to λ^3 for $\lambda \gg 1$. Our experimental data fully cover the quadratic regime of ζ_R and show the cross over to the third-power regime for $\lambda > 1$. Remarkably, these results are different from those obtained using active microrheology in oil (PDMS) films [10], where the agreement with the Levine's theory was significantly poorer, especially in the range of small λ. This discrepancy was attributed to the compressibility of the oil layer on a fluid substrate and the flow of the oil over the inclusion. In the case of smectic films, however, the film is nearly incompressible and a change of the film thickness in response to a compressive stress may occur only through the nucleation of dislocations. The latter can be excluded in our experiment.

The meniscus around the inclusion is composed of a complex layer structure featuring regular arrangements of topological defects and dislocations on a microscopic scale. This inhibits flow within the decorated regions around the inclusions. At the same time, the film outside the meniscus is perfectly uniform and flat on the hydrodynamic scale, so that there is no influence of potential curvatures on the viscous dynamics [26,27].

In summary, we reported an experimental study of translational and rotational viscous drag coefficients for rod-shaped inclusions in an isotropic quasi-2D fluid, modeled by a freely suspended liquid crystal film. The drag coefficients show a distinct nonlinear dependence on the rod size. The translational drag exhibits an anisotropic behavior already for the smallest aspect ratios and is in an excellent agreement with the theory by Levine *et al.* [24]. Immobile meniscus has to be accounted for in the effective size of the inclusion. We confirm a crossover behavior of the translational drag coefficient, $\zeta_\perp$, to a regime where the drag is purely local and depends linearly on the length L. For sufficiently small lengths $L \ll L_s$, the translational drag coefficients can be well described by the thin-rod approximation.

Notably, the *transversal* mobility of thin rods can be reasonably well described by the Petrov-Schwille equation, where the radius of an equivalent circular inclusion is taken as $L/2$. The enormous aspect ratio of freely suspended smectic films in combination to the easy adjustment of homogeneous film thicknesses from nanometers to micrometers allowed quantitative measurements of the diffusion of rods over more than three orders of magnitude in the effective rod length λ, which is hardly achievable with any other physical system.

ACKNOWLEDGMENTS

The authors acknowledge funding by Deutsche Forschungsgemeinschaft (DFG) within Project No. STA 425/28-1 and C.K. acknowledges a Landesstipendium Sachsen-Anhalt. We are indebted to J. E. Maclennan (University of Colorado) for fruitful discussions.

[1] K. Simons and E. Ikonen, Functional rafts in cell membranes, Nature **387**, 569 (1997).
[2] R. Stein, E. J. Hustedt, J. V. Staros, and A. H. Beth, Rotational dynamics of the epidermal growth factor receptor†, Biochemistry **41**, 1957 (2002).
[3] J. Schweizer, M. Loose, M. Bonny, K. Kruse, I. Monch, and P. Schwille, Geometry sensing by self-organized protein patterns, Proc. Natl. Acad. Sci. USA **109**, 15283 (2012).
[4] P. Steffen, P. Heinig, S. Wurlitzer, Z. Khattari, and Th. M. Fisher, The translational and rotational drag on langmuir monolayer domains, J. Chem. Phys. **115**, 994 (2001).
[5] K. Weiß, A. Neef, Q. Van, S. Kramer, I. Gregor, and J. Enderlein, Quantifying the diffusion of membrane proteins and peptides in black lipid membranes with 2-focus fluorescence correlation spectroscopy, Biophys. J. **105**, 455 (2013).
[6] M. Poo and R. A. Cone, Lateral diffusion of rhodopsin in the photoreceptor membrane, Nature **247**, 438 (1974).
[7] B. D. Hughes, B. A. Pailthorpe, and L. R. White, The translational and rotational drag on a cylinder moving in a membrane, J. Fluid Mech. **110**, 349 (1981).
[8] Y. Gambin, R. Lopez-Esparza, M. Reffay, E. Sierecki, N. S. Gov, M. Genest, R. S. Hodges, and W. Urbach, Lateral mobility of proteins in liquid membranes revisited, Proc. Natl. Acad. Sci. USA **103**, 2098 (2006).
[9] A. Anguelouch, R. L. Leheny, and D. H. Reich, Application of ferromagnetic nanowires to interfacial microrheology, Appl. Phys. Lett. **89**, 111914 (2006).
[10] M. H. Lee, C. P. Lapointe, D. H. Reich, K. J. Stebe, and R. L. Leheny, Interfacial hydrodynamic drag on nanowires embedded in thin oil films and protein layers, Langmuir **25**, 7976 (2009).
[11] P. G. Saffman, Brownian motion in thin sheets of viscous fluid, J. Fluid Mech. **73**, 593 (1976).

[12] P. G. Saffman and M. Delbrück, Brownian motion in biological membranes, Proc. Natl. Acad. Sci. USA **72**, 3111 (1975).
[13] E. P. Petrov and P. Schwille, Translational diffusion in lipid membranes beyond the Saffman-Delbruck approximation, Biophys. J. **94**, L41 (2008).
[14] Z. H. Nguyen, M. Atkinson, C. S. Park, J. E. Maclennan, M. Glaser, and N. Clark, Crossover Between 2D and 3D Fluid Dynamics in the Diffusion of Islands in Ultrathin Freely Suspended Smectic Films, Phys. Rev. Lett. **105**, 268304 (2010).
[15] A. Eremin, S. Baumgarten, K. Harth, R. Stannarius, Z. Nguyen, A. Goldfain, C. Park, J. E. Maclennan, M. Glaser, and N. Clark, Two-Dimensional Microrheology of Freely Suspended Liquid Crystal Films, Phys. Rev. Lett. **107**, 268301 (2011).
[16] P. Cicuta, S. L. Keller, and S. L. Veatch, Diffusion of liquid domains in lipid bilayer membranes, J. Phys. Chem. B **111**, 3328 (2007).
[17] P. C. Magusin and M. A. Hemminga, A theoretical study of rotational diffusion models for rod-shaped viruses. The influence of motion on 31P nuclear magnetic resonance line shapes and transversal relaxation, Biophys. J. **64**, 1851 (1993).
[18] H. A. Stone and H. Masoud, Mobility of membrane-trapped particles, J. Fluid Mech. **781**, 494 (2015).
[19] M. Doi and S. F. Edwards, *The Theory of Polymer Dynamics* (Oxford University Press, New York, 1994).
[20] Alex J. Levine and F. C. MacKintosh, Dynamics of viscoelastic membranes, Phys. Rev. E **66**, 061606 (2002).
[21] M. M. Tirado, C. L. Martínez, and J. G. de la Torre, Comparison of theories for the translational and rotational diffusion coefficients of rodlike macromolecules. Application to short DNA fragments, J. Chem. Phys. **81**, 2047 (1984).
[22] M. Selmi, J. C. Loudet, P. V. Dolganov, T. Othman, and P. Cluzeau, Structures in the meniscus of smectic membranes: The role of dislocations? Soft Matter **13**, 3649 (2017).
[23] K. Harth, B. Schulz, C. Bahr, and R. Stannarius, Atomic force microscopy of menisci of free-standing smectic films, Soft Matter **7**, 7103 (2011).
[24] A. Levine, T. Liverpool, and F. MacKintosh, Dynamics of Rigid and Flexible Extended Bodies in Viscous Films and Membranes, Phys. Rev. Lett. **93**, 038102 (2004).
[25] A. J. Levine, T. B. Liverpool, and F. C. MacKintosh, Mobility of extended bodies in viscous films and membranes, Phys. Rev. E **69**, 021503 (2004).
[26] B. A. Camley and F. L. H. Brown, Contributions to membrane-embedded-protein diffusion beyond hydrodynamic theories, Phys. Rev. E **85**, 061921 (2012).
[27] R. G. Morris and M. S. Turner, Mobility Measurements Probe Conformational Changes in Membrane Proteins due to Tension, Phys. Rev. Lett. **115**, 198101 (2015).